

Original Research

Correlation Analysis of the Spatial Characteristics and Influencing Factors of the Block-Scale Thermal Environment: A Case Study in Jinan, China

Jiayun Wang¹, Fei Meng^{1*}, Tingting Jing², Lifan Qi¹

¹School of Surveying and Geo-Informatics, Shandong Jianzhu University, Jinan 250101, China

²School of Surveying, Mapping and Spatial Information, Shandong University of Science and Technology, Qingdao 266000, China

Received: 1 September 2024

Accepted: 28 October 2024

Abstract

As an important factor in urban planning and urban design, blocks exhibit complex and diverse thermal environment characteristics due to the thermal properties of the underlayment materials and the non-uniformity of the spatial distribution of the buildings. Previous research has predominantly concentrated on the urban-scale thermal environment and its underlying drivers. Yet, there remains a notable inadequacy in the precise identification of core urban heat island patches and critical nodes, the scientific rigor applied in selecting geographical units and research methodologies, as well as the depth of exploration concerning improvement strategies for the thermal environment at the block scale. To address this gap, this study uses a typical urban neighborhood in Jinan as a case study. It employs geographic information system (GIS), spatial statistics, and analysis methods, grounded in the spatial heterogeneity of different geographical units, to explore the spatial distribution characteristics and heterogeneity mechanisms of the thermal environment at the neighborhood scale. The results indicate that: (1) in the study area, the core area and the edge area account for the largest proportion of the heat island landscape, and the accumulation, diffusion, and radiation of the two areas lead to the increasing degree of aggregation among the heat island patches, which has an important impact on the adjustment balance of the heat environment inside the block and the spatial distribution pattern of the heat island. (2) There are significant differences in the correlation and explanatory power between urban form indicators and the land surface temperature (LST) among different geographical units. Local climate zoning (LCZ) can preserve the complete urban landscape type and has strong explanatory power for local thermal environmental effects, making it highly suitable for the block-scale analysis of thermal environmental spatial feature correlations. (3) The HRE (height of roughness elements), BEI (building evenness index), and SVF (sky view factor) are the indicators that have the greatest impact on the LST. Building height, evenness, and openness have a significant impact on the spatial distribution pattern of heat islands. Urban planners should fully consider the impact mechanisms of the indicator factors to

minimize the LST. We believe that these findings can offer new theoretical foundations and practical pathways for the precise governance of urban heat island effects and the intelligent regulation of urban climates.

Keywords: block scale, geographical unit, heat island pattern, correlation analysis, urban planning

Introduction

In recent years, rapid urban development and continuous population growth have significantly changed the surface morphology and underlying surface characteristics of urban agglomerations [1], causing a series of climate-related and environmental problems [2], such as extreme heat waves, floods, storm surges, and ozone holes [3-5]. Climate change threatens the health of urban residents in a variety of ways; for instance, extremely high temperatures can induce respiratory system diseases and cardio-cerebrovascular diseases [6-8]. The Blue Book on Climate Change in China (2022) highlights that global warming continues, and China's warming rate has been higher than the global average over the same period; this is a sensitive area for global climate change [9]. Numerous studies have indicated that widespread exposure to high temperatures exacerbates health risks, impacting various diseases, vulnerable populations, and regions with differing climates [10]. Urban areas are more susceptible to thermal environmental issues, such as high temperatures and heat waves, due to their complex building environments and frequent human activities [11, 12]. Therefore, against the background of the rapid change of the global climate and the rising health risks faced by human populations, research on urban spatial planning in response to climate change and the internal mechanisms of thermal environmental regulation has become urgent on a global scale [13, 14].

Human activities in the urban canopy have formed complex surface types and building forms, which impact solar radiation and air movement at the urban and local scales and then change the spatial distribution patterns of the thermal environment [15, 16]. As the basic unit of urban planning and design, the internal thermal environmental characteristics of a block largely depend on its own spatial structure. Morphological factors, including building height, sky view factor, and street aspect ratio, significantly influence the surface radiation energy balance and air circulation, collectively shaping the thermal environment within urban blocks. This results in a highly heterogeneous and complex thermal field pattern [17, 18]. Furthermore, the spatial spillover effects observed among urban blocks, in conjunction with their distinct differences in spatial locations and architectural morphologies, considerably impact the absorption efficiency of solar radiation, as well as the transportation and redistribution of water vapor and heat. These factors further exacerbate the complexity and heterogeneity of the thermal environment within these blocks [19, 20]. Thus, systematically analyzing how

the spatial morphological distribution characteristics of urban blocks precisely shape and regulate LST can contribute to elucidating the formation mechanisms of urban thermal environment heterogeneity. It also provides valuable insights into enhancing urban climate suitability, optimizing urban landscape patterns, and formulating scientifically rational urban planning strategies.

Geographical unit division is an important foundation for quantifying the spatial forms of urban blocks and the mechanisms of thermal environmental interactions. Numerous studies have extensively adopted geographical unit frameworks such as grids and LCZ to delve into the correlation between urban thermal environment and multi-dimensional influencing factors [21, 22]. The grid approach, leveraging professional GIS software like ArcGIS, constructs regularly spaced fishnet spatial units that are frequently utilized as fundamental units to investigate the scale effects of urban thermal environments. The homogenization of these units facilitates the exposition of both the similarities and complexities in thermal environments across diverse regions, enabling a nuanced dissection of urban thermal environment effects [23]. LCZ is a natural geographic unit comprehensively defined based on factors such as building layout, land cover characteristics, spatial morphology, and human activity intensity. It is capable of accurately reflecting the temperature distribution features and variation patterns among different land surface types [24]. The introduction of the LCZ framework significantly enhances the precision of urban thermal environment research, enabling in-depth insights into the impact of urban spatial structure on local climatic conditions. This framework provides robust support for the quantitative assessment, causal analysis, and formulation of mitigation strategies related to urban heat island effects [25, 26].

Researchers have developed a series of LCZ classification methods using remote sensing images and geographic information data. Bechtel et al. proposed the World Urban Database and Access Portal Tool (WUDAPT) [27], which utilizes Landsat remote sensing images and the Google Earth cloud platform to achieve rapid mapping; this method has been used widely in multiple urban areas, such as Beijing and Guangdong [28, 29]. However, due to the difficulty in meeting the quantity requirements of machine learning in extracting training samples at the medium and micro scale, the accuracy of LCZ-type recognition is low. Therefore, the WUDAPT method is more suitable for drawing LCZ at the large-scale level of cities [30]. LCZ classification needs to consider the building height,

land cover, sky openness, and other factors. Compared with remote sensing images, geographic information data can provide finer urban spatial form information [31]. Therefore, GIS-based methods can produce more accurate classification results within urban blocks [32]. Many scholars have attempted to use high-resolution remote sensing images and urban 3D building databases to calculate LCZ classification indicators using GIS methods. Many cities, such as Tokyo, Hong Kong, and Atlanta, have adopted this fine-grained classification method [33, 34]. However, GIS methods typically require accurate, complete, and real-time-updated city datasets, which are expensive to obtain and not suitable for all cities. Focusing on the problem of the difficulty of obtaining urban LCZ classification data, this study attempts to quantitatively describe urban spatial morphological parameters based on open multi-source geographic information data, construct an LCZ classification system with urban blocks as the basic unit of analysis, and use the manually calibrated classification methods combined with physical parameter thresholds for LCZ mapping.

The urban heat island effect has emerged as a critical issue influencing urban climate, public health, and ecosystem services, garnering significant attention in recent years. Despite substantial research on urban thermal environments and their driving factors, there is an urgent need to accurately identify core heat island patches and critical nodes that significantly impact the heat island effect. Furthermore, existing studies are often constrained by data availability and empirical biases, lacking in-depth analysis of thermal environment response patterns across different geographical units and regression models. Finally, LCZ-related studies primarily focus on LCZ mapping methods at the urban scale and the spatiotemporal differentiation characteristics of thermal environments in different types of LCZ. Further studies are needed to consider planning strategies for thermal environmental improvement within LCZ schemes at the block scale. In this context, the representative area of the Jinan High-Tech Zone serves as an example, employing multi-source remote sensing data and spatial statistical analysis methods to systematically explore the complexity and heterogeneity of urban thermal environments at the street block scale. Specifically, this study aims to: (1) Utilize the Morphological Spatial Pattern Analysis (MSPA) method to conduct a thorough examination of the spatial distribution characteristics of LST at the block scale, identifying and quantifying the core patches and critical nodes that significantly contribute to the urban heat island effect; (2) Reveal the differences and applicability of thermal environment response patterns at the street block scale through comparative analysis of various geographical units and regression models, thereby providing a scientific basis for precise modeling; (3) Further investigate the regulatory mechanisms of spatial morphological elements, such as building layout and underlying surface characteristics within street

blocks, on LST, thereby offering theoretical support for developing effective strategies for thermal environment mitigation and urban planning.

Material and Methods

Study Area

Jinan (36°01'–37°32' N, 116°11'–117°44' E) is located in the middle of the North China Plain, a region with a warm temperate continental monsoon climate; in summer, it is one of the hottest cities in China. With the rapid expansion of the city, the increase in population concentration, and the limited space available for construction planning and development, the urban heat island effect is intensifying. This study selects the typical central business district (CBD) of the Jinan high-tech zone as the research area; this district has an area of approximately 11 km². There is a wide range of building types in the region, including a series of functional areas such as commercial areas, residential areas, industrial areas, scenic areas, cultural and educational areas, etc. The land-cover types are diverse, including ecological forests, parks, lakes, soil, asphalt surfaces, etc. The unique architectural spatial pattern within the region produces different microclimate characteristics, which facilitate an analysis of the spatial heterogeneity of the local geothermal environment and have strong research value and practical significance (Fig. 1).

Datasets

The data mainly comprise: (1) remote sensing image data and (2) geographic information data. The remote sensing image data include Landsat8 images, ZY-3 images, and Google Earth image data. The geographic information data includes data related to the DEM, 3D buildings, road networks, and administrative divisions. See Table 1 for details.

Methodology

The Block Spatial Form Indicator System

As the smallest control unit of the urban microclimate, a block's spatial structure composition and configuration have a significant impact on the thermal environment. This study references conclusions related to factors influencing thermal environments [35-37] and, drawing on the data foundation of this research, selects eight spatial morphological indicators for cities based on the principles of generalizability, applicability, and representativeness, aiming to comprehensively reflect the structural composition and spatial configuration of the study blocks (Table 2). In terms of the 2D land cover, the types and proportions of the underlying surfaces are closely related to differences in the urban microclimate; these indicators include the impervious surface fraction

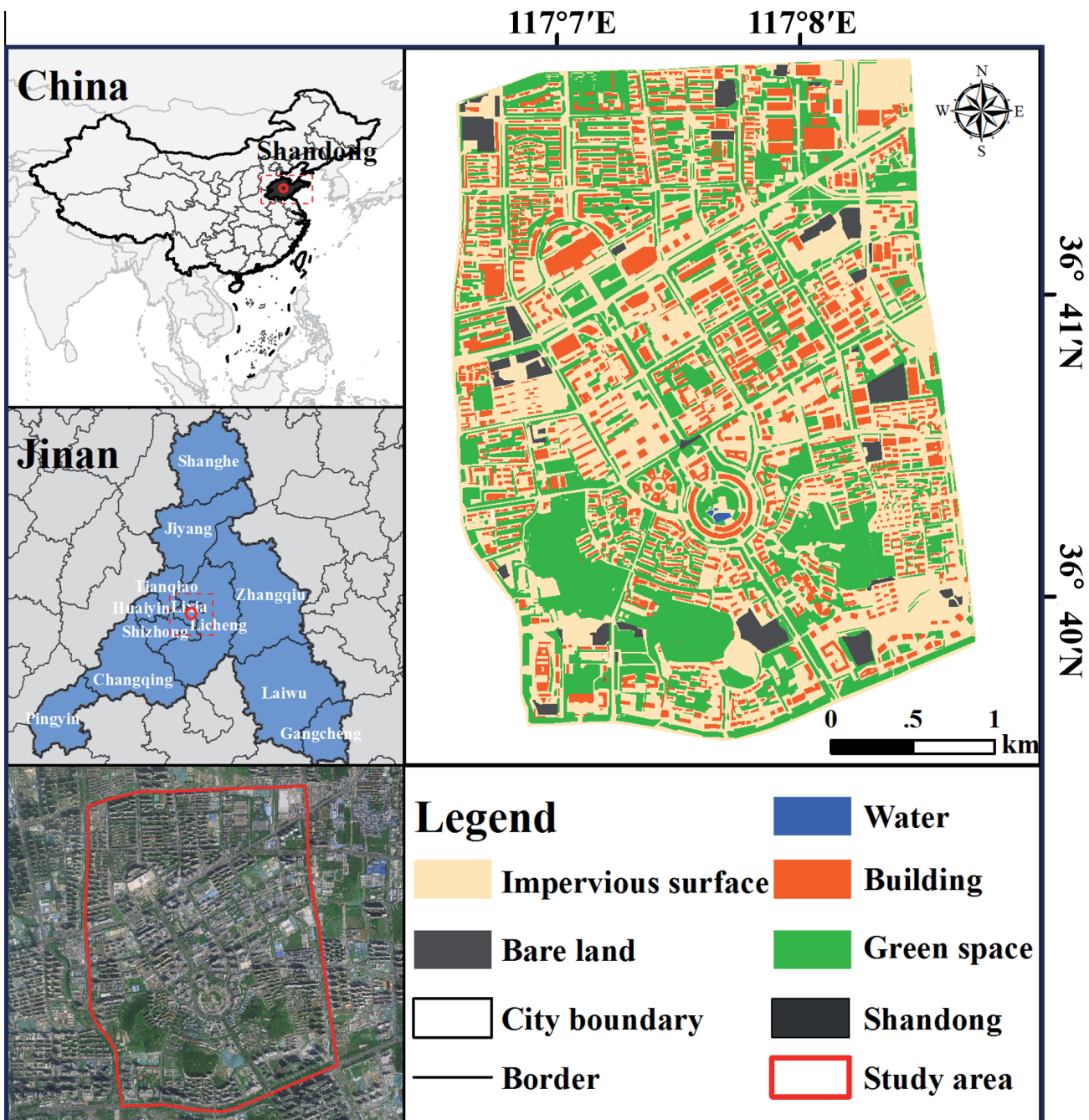


Fig. 1. Study area.

(ISF) and the pervious surface fraction (PSF). The ISF represents the proportion of impervious surfaces (hard paving such as asphalt, marble, brick, etc.). The PSF represents the proportion of pervious surfaces (soil, vegetation, water, etc.). In terms of 3D spatial forms, the indicators include the spatial crowding degree (SCD), average building volume (AV), building evenness index (BEI), height of roughness elements (HRE), height coefficient of variation (CH), and sky view factor (SVF). The SCD and BEI, respectively, represent the crowding and evenness of buildings in 3D space, the AV represents the average volume of buildings, the HRE and CH are important parameters for characterizing

height characteristics, and the SVF is the ratio of the visible sky area to the total sky area at a point in space [38].

LCZ Mapping

According to Stewart and Okay's definition, LCZs can be categorized into 17 standard types, including 10 "building types" (LCZ1–10) and 7 "land-cover types" (LCZA–G) [24]. The reference basis for LCZ mapping is relatively complex. In order to avoid errors in the building density, height, and surface coverage causing incorrect LCZ classifications, this article adopts physical

Table 1. Data source information description.

Name	Date	Data role	Data source
Landsat8 image	2021.8.15	Land surface temperature retrieval	Geospatial Data Cloud (www.gscloud.cn)
ZY-3 image	2021.5.17	Land-use classification	Environmental Monitoring Station
Google Earth image	2021	LCZ drawing reference	Google Earth (earth.google.com)
DEM data	2021	Urban spatial form parameter calculation	Geospatial Data Cloud (www.gscloud.cn)
3D building data	2021	Contains building contour and height information for obtaining the 3D shape data of buildings	Water Flow Micromap Software (www.rivermap.cn)
Road network data	2021	Dividing block units based on road network data for LCZ mapping	Shandong Provincial Sky Map (www.sdmap.gov.cn)
Administrative division data	2021	Study area division and remote sensing image cropping	Shandong Provincial Sky Map (www.sdmap.gov.cn)

parameter thresholds [39] combined with manual calibration methods to classify LCZ categories; these physical parameters include the SVF, HRE, PSF, and ISF. The calculation steps are as follows: (1) divide the study area into blocks of different sizes based on road network data. (2) Using 3D building and surface cover data, calculate the urban spatial form and preliminarily establish the LCZ type based on physical parameter thresholds. (3) Verify the findings through manual visual methods and correct the classification types of urban blocks to obtain the final LCZ classification results.

The LCZ classification results are shown in Fig. 2. The study area is mainly composed of building-based LCZ types, with a proportion of up to 81.22%. Among

them, the type with the highest proportion is open high-rise LCZ4, followed by open middle-rise LCZ5 and open low-rise LCZ6. The proportion of dense building areas (LCZ1~LCZ3) is only 4.60%, and other building types are scattered among them. The proportion of LCZs with the surface-cover type is 18.78%, with the highest proportion comprising LCZE, which is composed of exposed rocks or hard pavement and is mainly distributed in the road square areas of the study area. The second most common type is the dense forest landscape area LCZA, which is mainly distributed in forest parks in the southern part of the study area. LCZC/D accounts for a relatively small proportion and

Table 2. Urban spatial form indicator system.

Indicator	Formula	Data methods	Description
PSF	$PSF = \frac{Area_{pervious}}{Area_{total}}$	ArcGIS, pervious surface vector data	$Area_{pervious}$ represents the coverage area of the impervious surface, $Area_{total}$ represents the total area of the study area.
ISF	$ISF = \frac{Area_{impervious}}{Area_{total}}$	ArcGIS, impervious surface vector data	$Area_{impervious}$ represents the coverage area of the pervious surface.
AV	$AV = \frac{1}{n} \sum_{i=1}^n V_i$		V_i represents the volume of the i^{th} building in the study area, n represents the number of buildings in the study area.
SCD	$SCD = \frac{\sum_{i=1}^n V_i}{H_{max} \times Area_{total}} \times 100(\%)$		H_{max} represents the maximum height of the buildings in the study area.
BEI	$BEI = \sqrt{\frac{\sum_{i=1}^n (V_i - AV)^2}{Area_{total}}}$	ArcGIS, 3D building data	AV represents the average building volume within the study area.
HRE	$HRE = \frac{1}{n} \sum_{i=1}^n H_i$		H_i represents the height of the i^{th} building in the study area.
CH	$CH = \frac{1}{HRE} \left[\frac{1}{n} \sum_{i=1}^n (H_i - HRE)^2 \right]^{\frac{1}{2}}$		HRE represents the average building height of the study area.
SVF	$SVF = \frac{Area_{sky}}{Area_{total}}$	SAGA-GIS, DEM, 3D building data	$Area_{sky}$ represents the visible sky area.

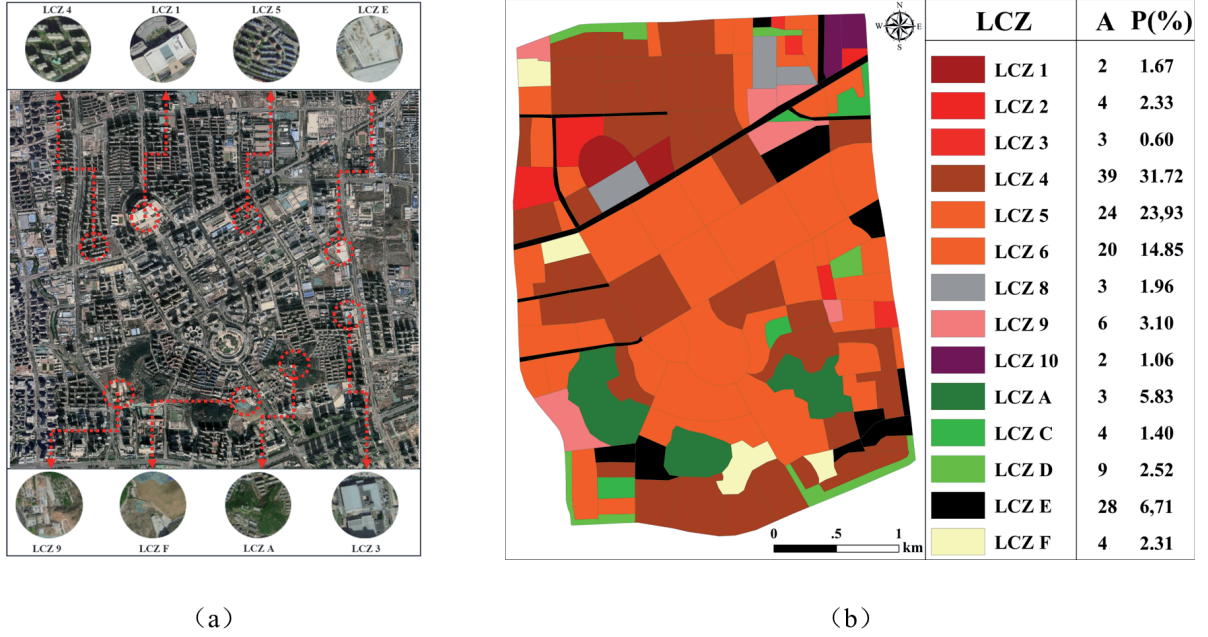


Fig. 2. LCZ mapping reference example. (a) Example of LCZ types; (b) LCZ mapping results.

is mainly distributed in the grassland landscape areas at the edges of roads.

Land Surface Temperature Inversion

This study uses the radiation equation algorithm to invert the land surface temperature [40]. The principle is to subtract the total amount of radiation received by the sensor from the amount of radiation affected by the atmosphere to obtain the surface heat radiation intensity; then, we convert the heat radiation intensity into the true surface temperature. The thermal infrared radiation transfer equation is expressed as:

$$L(\lambda) = \tau[\varepsilon B(T_s) + (1 - \varepsilon)L_{atm\downarrow}] + L_{atm\uparrow} \quad (1)$$

where $L(\lambda)$ is the radiation brightness on the star ($W \times m^{-2} \times \mu m^{-1} \times sr^{-1}$), τ is the spectral atmospheric transmittance, ε is the surface specific emissivity, T_s is the land surface temperature (K), B is the Planck function, and $L_{atm\uparrow}$ and $L_{atm\downarrow}$ are the atmospheric upward radiation and atmospheric downward radiation, respectively ($W \times m^{-2} \times \mu m^{-1} \times sr^{-1}$).

When the surface emissivity has been determined, the land surface temperature T_s is obtained according to Planck's formula:

$$T_s = K_2 / \ln(K_1 / B(T_s) + 1) \quad (2)$$

where K_1 and K_2 are radiation constants. For Landsat8 TIRS data, $K_1 = 774.89$ ($W \times m^{-2} \times \mu m^{-1} \times sr^{-1}$), $K_2 = 1321.08K$.

Correlation Analysis

(1) Spatial autocorrelation analysis

This study used spatial autocorrelation analysis to test the spatial correlation of the LST, including the Global Moran's I and Local Moran's I. The Global Moran's I is used to test the spatial aggregation degree and spatial dependence of LST [41], represented by equation (3) as:

$$I = \frac{\sum_{i=1}^n \sum_{j=1}^n w_{ij} (x_i - \bar{x})(x_j - \bar{x})}{S^2 \sum_{i=1}^n \sum_{j=1}^n w_{ij}} \quad (3)$$

where n represents the number of pixels in the study area, x_i and x_j represent the LSTs of pixels i and j , respectively, \bar{x} is the mean of all pixels in the study area, w_{ij} is the spatial weight matrix, and S is the standard deviation. The I range is between -1 and 1. When $I > 0$, it indicates a positive spatial correlation, with larger values representing a more significant spatial correlation. When $I < 0$, it indicates a negative spatial correlation, with smaller values indicating greater spatial differences. When $I = 0$, it indicates a random distribution.

The Local Moran's I was used in this study to further test the hot spots, cold spots, and spatial outliers with statistical significance in the local region [42]. It is expressed by equation (4):

$$I_L = \frac{\sum_{i=1}^n \sum_{j=1}^n w_{ij} (x_i - \bar{x})(x_j - \bar{x})}{S^2} \quad (4)$$

(2) Spatial regression analysis

Spatial regression analysis considers the spatial relationships of the research object. It can eliminate the problem of spatial dependency between data samples and allow us to accurately analyze the correlation between the LST and its influencing factors [35]. The spatial regression model includes the spatial error model (SEM) and the spatial lag model (SLM). The SEM is represented by Equation (5) as:

$$y = x\beta + \lambda w_u + \varepsilon, \quad \varepsilon \sim N(0, \delta^2) \quad (5)$$

where y represents the dependent variable matrix, x represents the independent variable matrix, β represents the parameter matrix, λ represents the regression coefficient of the spatial residual term, w_u represents the spatial adjacency weight matrix, and ε represents the vector of the spatial error term.

SLM is represented by Equation (6) as:

$$y = \rho w_y + x\beta + \varepsilon, \quad \varepsilon \sim N(0, \delta^2) \quad (6)$$

Where y represents the dependent variable matrix, x represents the independent variable matrix, w_y represents the spatial weight matrix, ρ represents the autoregressive parameter, β represents the coefficient vector, and ε represents the vector of the spatial error term.

Morphological Spatial Pattern Analysis

MSPA is an image processing method based on mathematical morphology; it is used to measure, recognize, and describe raster images [43]. In this study, the MSPA model was applied to urban heat island analysis. First, ArcGIS was used to classify the heat island intensity [44] and convert it into binary TIFF data, taking the heat island area as the foreground and the non-heat island area as the background; then, MSPA analysis was performed on binary TIFF images using

GTB software. The MSPA type definition is shown in Table 3.

Framework Description of this Study

We divided the study area into two types of geographical units—LCZs and fishnets—and used the GIS spatial analysis method to explore the impact mechanism of urban spatial form on LST at the block scale. The basic steps are as follows: (1) extracting urban spatial form indicators based on the units of the LCZ and the fishnet. Based on image resolution and existing research conclusions [45, 46], the optimal spatial scale for fishnets was set to 150m × 150m. (2) We used Pearson correlation analysis and a multicollinearity test to screen eight urban spatial form indicators to establish the best indicator system. (3) We tested the global correlation between the LST and the spatial form indicators based on the OLS model and calculated Moran's I for the residuals in the model operation results. If Moran's I was significant, we used spatial regression models to continue exploring the spatial relationship between them. If Moran's I was not significant, we used the OLS model to analyze the global relationship. (4) Based on the R², LM test, Robust LM test, Log Likelihood, and AIC parameter information in the model, the optimal study unit (LCZ or fishnet) and spatial regression model (SEM or SLM) were selected for a correlation analysis of the block-scale thermal environment spatial features (Fig. 3).

Results and Discussion**Pearson Correlation Analysis**

This study employed the Pearson correlation coefficient to examine the relationship between urban spatial form indicators and LST, as depicted in Fig. 4. The analysis reveals notable variability in these correlations across different geographical units.

Table 3. Definition of landscape types in MSPA.

MSPA type	Ecological implications
core	The pixel set with foreground pixels larger than the specified edge width, as the "source" of various ecological processes, plays an important role in maintaining the urban ecological environment.
islet	Plaques that are not connected to any foreground area have a lower possibility of internal material and energy exchange and transmission.
loop	The foreground data connected to the core area have corridor properties, which can enhance the material circulation and energy flow inside the core area.
bridge	The channel connecting adjacent core areas, with corridor properties, is a channel for energy flow and material exchange.
perforation	The transition zone between the core area and its internal non-core area has edge effects.
edge	The edge outside the foreground is the transition area between the periphery of the core area and different landscape elements.
branch	The area where only one end of the branch line is connected to the edge, bridge, loop, or perforation.

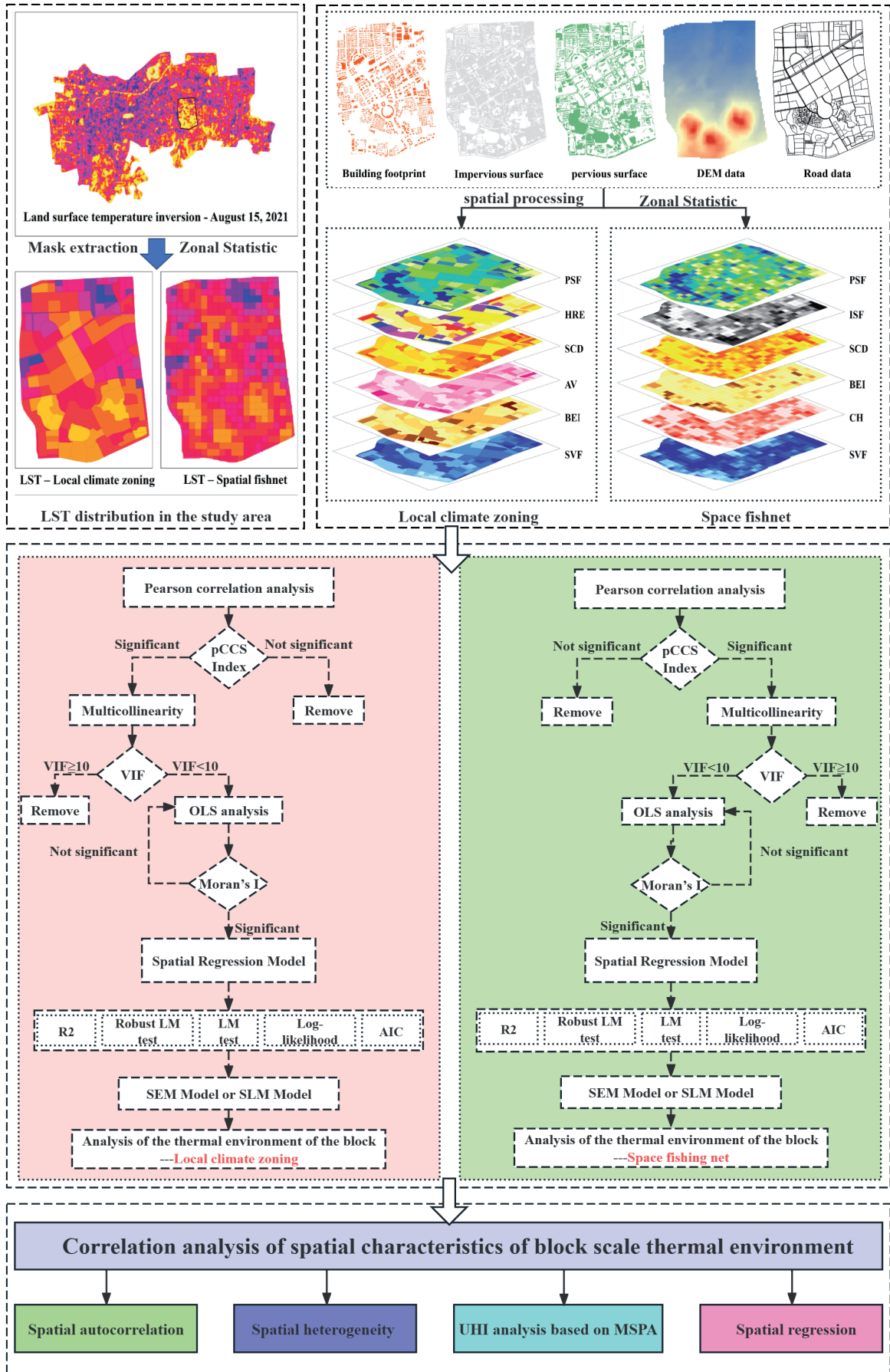


Fig. 3. Study framework.

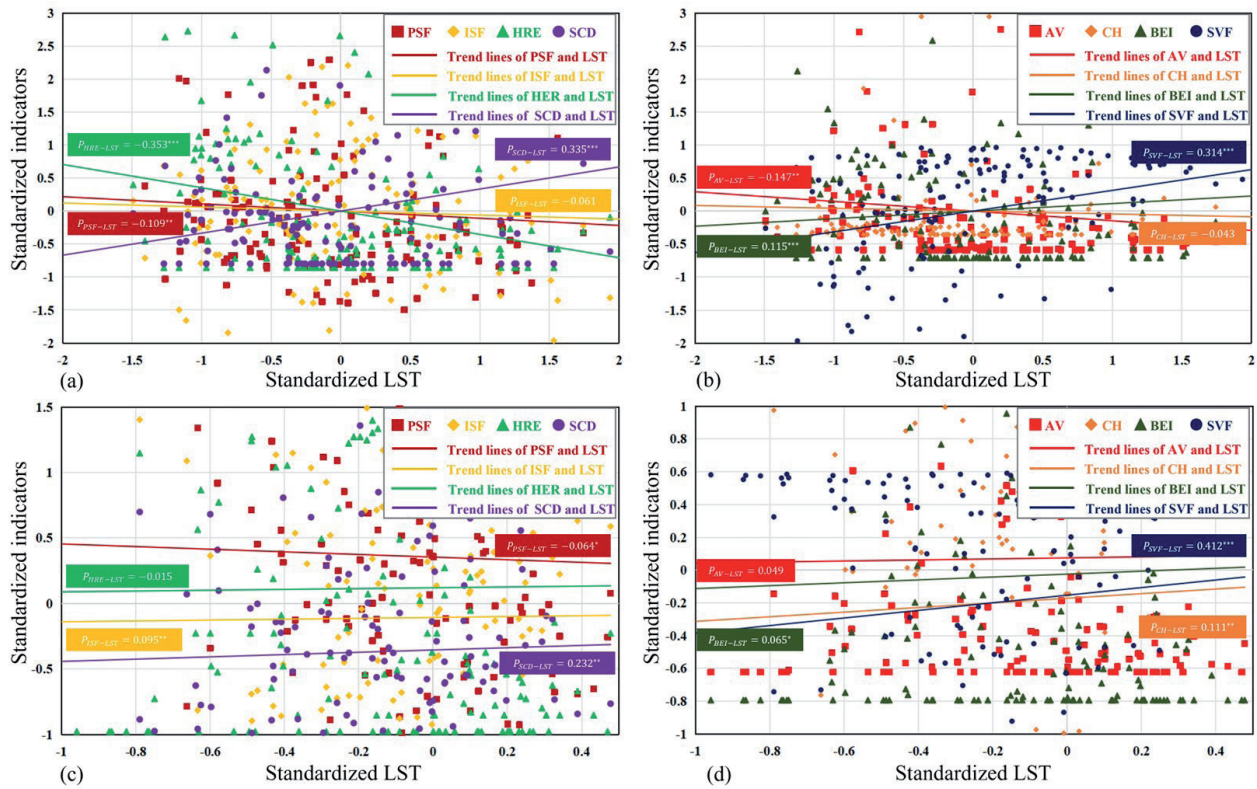


Fig. 4. Correlation analysis between spatial indicators and LST. (a)PSF, ISF, HRE, SCD in LCZ; (b)AV, CH, BEI, SVF in LCZ; (c)PSF, ISF, HRE, SCD in Fishnet; (d)AV, CH, BEI, SVF in Fishnet. Note: *** $p < 0.01$, ** $p < 0.05$, * $p < 0.1$

Generally, stronger correlations between urban spatial morphology indicators and LST were observed in LCZ units. PSF exhibited a negative correlation with LST in both LCZ and fishnet units. This underscores the role of permeable surfaces in reducing LST by enhancing latent heat loss through surface moisture evaporation and increased water evaporation and heat exchange. Conversely, ISF characterizes the proportion of urban impervious surface coverage and showed a strong correlation with LST in fishnet units but did not achieve significance in LCZ. This discrepancy may be attributed to LCZ classification accounting for construction and human activities, which can diminish ISF explanatory power regarding LST. BEI positively correlated with LST in LCZ and fishnet units, indicating that a uniform distribution and orientation of buildings facilitate air convection, thus dissipating heat and lowering LST. SCD and SVF demonstrated significant positive correlations with LST in both LCZ and fishnet units. These indicators influence wind speed, heat circulation, and surface radiation intensity, exacerbating UHI effects. HRE and AV exhibited significant correlations with LST in LCZ (negative for HRE and positive for AV), but these correlations were not significant in fishnet units ($p > 0.1$). This disparity may arise from grid boundaries affecting building fragmentation and thereby weakening the explanatory power of these factors on thermal environment effects. Moreover, CH displayed

a significant positive correlation with LST in fishnet units but did not pass the significance test in LCZ. This distinction could be due to the finer spatial division of fishnet units, enabling greater differentiation in building heights within the same grid and facilitating stronger correlations. In contrast, LCZ covers larger geographic areas with more complex variations in building heights, resulting in a lower and more varied correlation. In summary, these findings emphasize the subtle impact of urban spatial forms in different geographic units on LST, therefore, localized methods are needed in urban planning to effectively mitigate the effects of heat islands.

Model Performance Parameter Analysis

Multicollinearity Test

According to the PCCs shown in Fig. 4, we selected indicators that pass the significance test ($p \leq 0.1$) to construct a multiple regression analysis model. Before building the model, multicollinearity tests were conducted on the significant indicators in the LCZ and fishnet models to ensure the stability of coefficient estimation in the regression model and the reliability of the hypothesis testing. First, we conducted the bivariate autocorrelation test on the indicators in SPSS [47]. Fig. 5a shows that no multicollinearity exists in

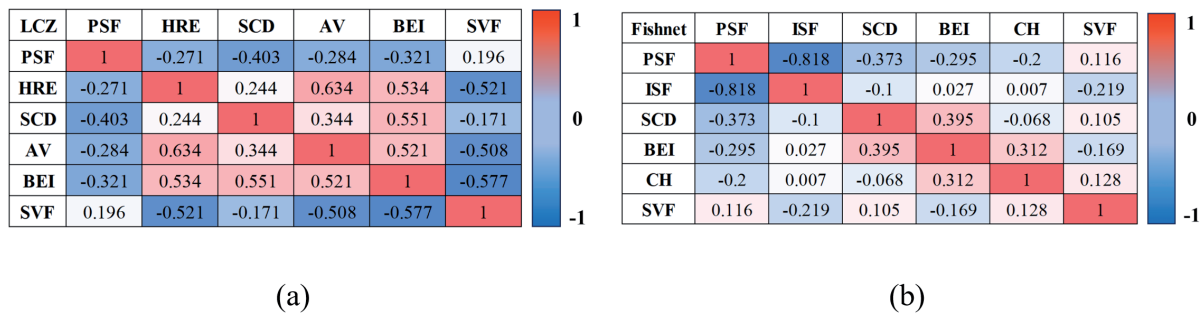


Fig. 5. Bivariate autocorrelation test results. (a) LCZ; (b) Fishnet.

the indicators in LCZ units ($|PCCs| < 0.7$), while Fig. 5b shows the significant negative correlation between PSF and ISF in the fishing net unit ($|PCCs| > 0.7$), indicating that there is a possibility of multicollinearity. Second, we used the variance inflation factor (VIF) in SPSS to conduct the multicollinearity test [48]. The threshold value was set to 10, and significant outlier factors ($VIF \geq 10$) were removed until the VIF value was stable and there was no large outlier ($VIF < 10$). The test results are shown in Table 4. The spatial form indicators in the LCZ units all passed the multicollinearity test, while the PSF in the fishnet units is significantly correlated with the ISF, indicating that there is strong multicollinearity. We deleted the PSF indicator with the largest VIF value and performed the multicollinearity test again. The VIF values of all indicators are less than 10. According to the test results, we constructed multiple regression models for the LCZ and fishnet units for the subsequent correlation analysis.

Comparative Analysis of Regression Models in Different Geographical Units

This study used different regression models for the correlation analysis of the LCZ and fishnet units, and the results are shown in Table 5. First, by comparing the impact of the geographical unit division methods on the analysis results, it can be seen that there are significant differences in the model's accuracy between the different geographical units. The LCZ has a stronger LST, which manifests as a higher R^2 and Log Likelihood and a lower AIC. This is because the LCZ unit can preserve the complete landscape types within the block and partition the thermal environment response

capacity based on the surface characteristics, fully reflecting the spatial heterogeneity between different LCZ types, thus producing more accurate analysis results. Next, comparing the impact of the regression models on the analysis results, the results show that the fitting accuracy of the spatial regression models is significantly better than that of the OLS models. At the same time, a significant spatial dependence was found in the OLS model analysis results (Moran's $I=0.360$), while SEM and SLM eliminated the autocorrelation of LST residuals through spatial autocorrelation modeling, with Moran's I values of 0.053 and 0.008, respectively. To determine which spatial regression model performs best, we comprehensively compared the performances of SLM and SEM from the perspectives of five parameters. The larger the R^2 , Log Likelihood, LM, and Robust LM values, the smaller the AIC, indicating better model performance. The results show that the parameters of SEM are better than those of SLM overall and are more suitable for the interpretation of the spatial differentiation of the surface temperature, which is consistent with the results of previous studies [49]. Therefore, we chose the LCZ as the research unit and the SEM model as the research method for analyzing the spatial correlation of thermal environmental characteristics at the block scale.

Correlation Analysis of the Spatial Characteristics of Block-Scale Thermal Environments Based on the LCZ

Spatial Characteristics Analysis of the LST

The LST distribution within the study area (Fig. 6a) exhibits significant spatial heterogeneity, with

Table 4. Multicollinearity test of spatial morphological indicators.

LCZ	PSF	HRE	SCD	AV	BEI	SVF
VIF	1.236	3.375	1.671	2.479	2.366	2.277
Fishnet	PSF	ISF	SCD	BEI	CH	SVF
VIF	14.235	11.658	4.429	1.519	1.992	1.183
Fishnet	PSF	ISF	SCD	BEI	CH	SVF
VIF	--	1.108	1.329	1.513	1.238	1.183

Table 5. Model performance parameters for different geographical units.

Geographic unit	LCZ			Fishnet		
	OLS	SLM	SEM	OLS	SLM	SEM
R ²	0.366	0.519	0.586	0.207	0.290	0.294
LM	---	57.777***	58.238***	---	45.264***	40.654***
Robust LM	---	5.169**	5.630**	---	4.722**	0.113
Log-likelihood	-234.694	-211.065	-210.673	-1419.430	-1397.860	-1398.028
AIC	504.462	438.13	435.347	2850.850	2809.710	2808.060
Moran's I	0.390	0.053	0.008	0.143	-0.010	-0.002

Note: ***p<0.01, **p<0.05, *p<0.1

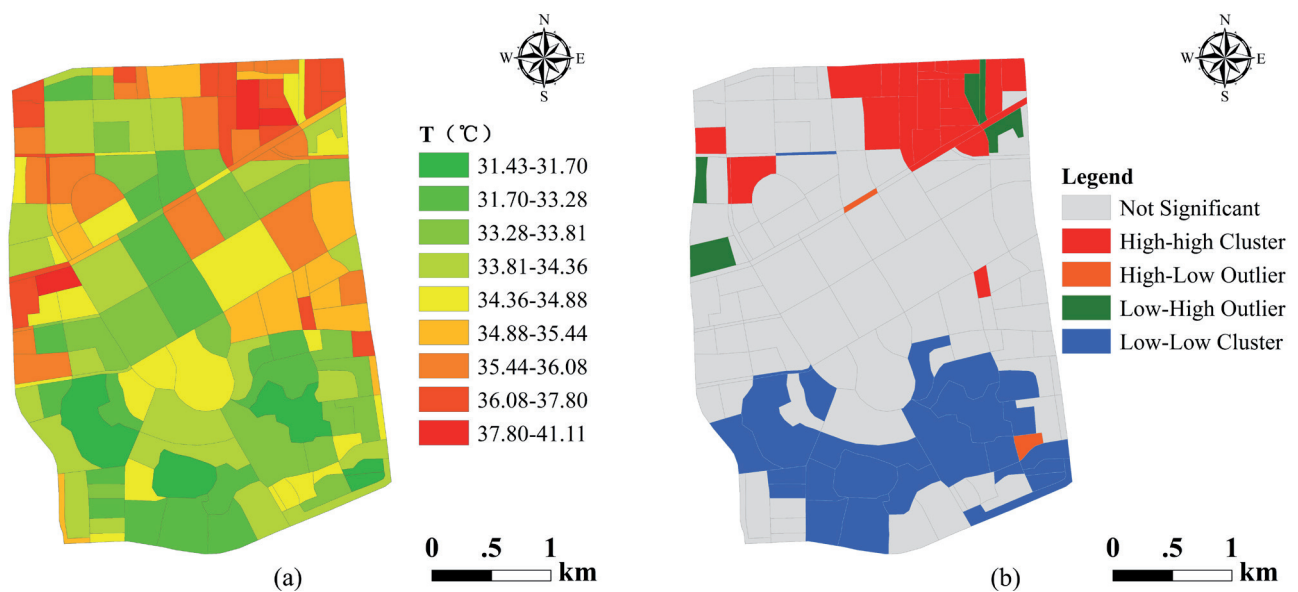


Fig. 6. LST spatial characteristics (a) Spatial distribution of LST; (b) LISA cluster map of LST.

a maximum temperature difference of 9.68 °C. The high-temperature areas are primarily concentrated in the industrial and commercial-intensive zones in the northeast, central, and western regions of the study area, with the main types being large, low-rise buildings. They consume a large amount of building energy and generate artificial heat sources, causing an increase in the surface temperature and an imbalance in thermal environmental regulation. The low-temperature areas are mainly concentrated in forest park scenic areas in the south, where large trees and other vegetation can produce cooling effects through transpiration and shading. The LISA aggregation map (Fig. 6b) is somewhat similar to the LST in terms of spatial distribution. A high–high cluster occurs in the northeast of the study area, and the surface is mainly covered by impervious surfaces such as asphalt and masonry. Due to the lack of shelter from high-rise buildings, the surface is directly exposed to strong solar radiation, forming a heat island cluster. In contrast, the high-rise building areas and vegetation-rich scenic forest areas in the south exhibit significant

low–low clusters, with the shadows of tall buildings and green vegetation effectively reducing the LST.

Based on MSPA, we further analyzed the distribution characteristics of the heat island cluster, and the results are shown in Fig. 7. The core area accounts for 54.77% of the heat island patch area, with an average LST of 36.75 °C, which is mainly concentrated in the central and northern regions of the study area, showing a trend of clustering and spreading in terms of the spatial distribution. The heat island area of the peripheral area is second only to that of the core area, with a proportion of 40.95%, with an average LST of 35.42 °C. This is because the edge area is a transition area between the periphery of the core area and different landscape elements, so the morphological distribution of the edge area is strongly affected by the spillover effect of the core area. The proportion of the heat island area comprising islets, bridges, perforations, branches, and loop types is only 4.28%. Based on the above research, we found that the core area and edge area account for the majority of the heat island patches in all types of

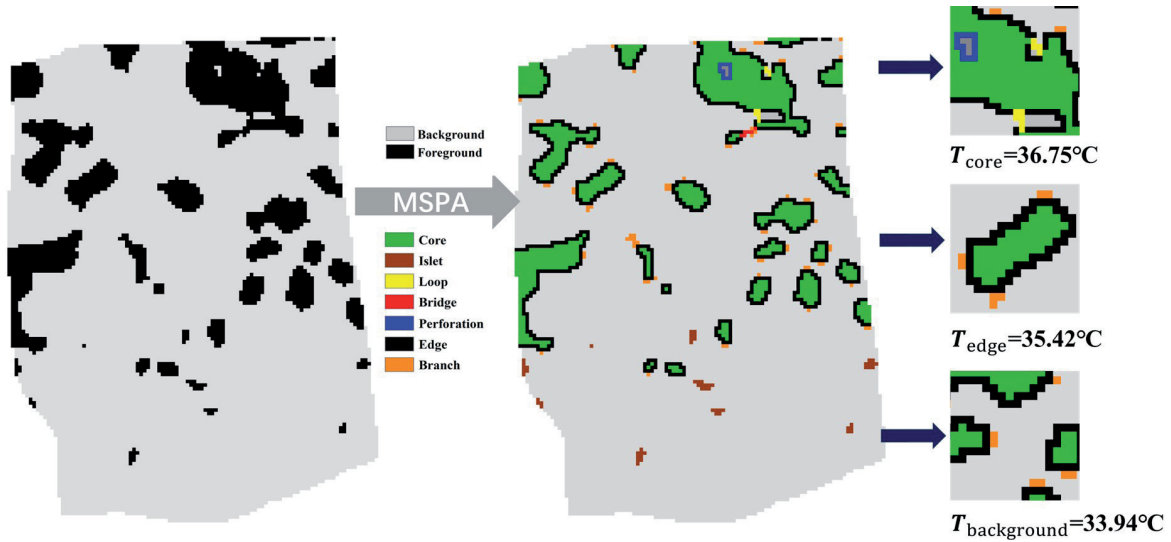


Fig. 7. MSPA classification results of heat island patches.

MSPA, which is an important factor that affects and changes the strength and stability of the UHI. As the "source" of urban heat island patches, the core area, through accumulation, diffusion, and radiation, leads to the increasing degree of aggregation among heat island patches, which has a significant impact on the balance of thermal environmental regulation and spatial distribution patterns. As the peripheral part of the core area edge, the edge area has the boundary attribute of an ecological landscape. Adjacent heat island patches penetrate and connect with each other through the edge area, promoting the circulation and transfer of heat, and further changing the spatial distribution patterns of the thermal environment.

Analysis of the LST in Different LCZ Types

To explore the differences in the LST between various LCZ types, we drew an LST box plot, as shown in Fig. 8. In the LCZs of building types, the average heat island intensity of high-density buildings (LCZ1~3) is higher than that of low-density buildings (LCZ4~LCZ6). High-density areas tend to form heat island clusters due to densely clustered buildings and reduced air circulation and heat transfer. High-rise buildings can alleviate the intensity of the heat island to a certain extent. Their building space structure has long and narrow street canyons (a small SVF) and large building shadows (a large HRE), which can not only reduce solar radiation and urban heat accumulation but also provide more shade, thus improving thermal comfort and reducing building energy consumption. Therefore, LCZ1 and LCZ4 exhibit lower LST values. LCZ8 and LCZ10 are mainly composed of large low-rise buildings (with higher SVF values and lower HRE values), with extremely low vegetation coverage; in these areas, the building materials are mostly reinforced concrete, stone, and glass curtain walls, so the heat island intensity is

the most pronounced. However, the sparse construction area (LCZ9) is mainly composed of scattered small and medium-sized buildings, with low grass and shrub vegetation distributed in the area and strong ground permeability, which can alleviate the heat island effect to a certain extent. Among the land cover types of LCZ, LCZA, and LCZC show lower LST values, with LCZA having the lowest heat island intensity. Green vegetation, dominated by dense forest trees, has a higher leaf area coverage rate, which can provide sufficient shade, transpiration, and heat absorption, forming a "cold island effect" and effectively reducing the surface temperature. The heat island intensity in the exposed sandy soil area of LCZF is the most significant, and an increase in soil exposure will exacerbate the soil heat exchange process, leading to an increase in the surface temperature [50]. LCZD low-vegetation areas exhibit high LST values due to a severe lack of shade, increased absorption of solar heat radiation, and the limited cooling effect provided by low vegetation, such as grasslands. LCZE is mainly composed of asphalt, marble, brick, and other hard pavements (the ISF is large); the building materials have high heat-absorption characteristics, and the warming effect is very obvious. However, this study found that the heat island intensity of LCZE was not significant, possibly because LCZE was mainly distributed across the urban roads in the study area, and trees, shrubs, and other types of green vegetation on both sides could provide a certain shade and cooling effect, reducing the heat island intensity to a certain extent.

The Comprehensive Impact of Urban Spatial Form Indicators on LST

Based on the SEM model, we analyzed the relative contribution of LCZ urban form indicators to the LST, as shown in Fig. 9. There is a significant negative correlation between HRE and LST, with a relative

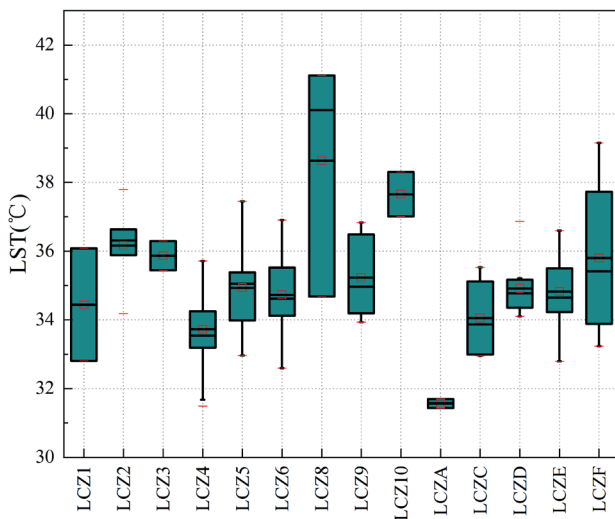


Fig. 8. LST boxplot for different LCZ types.

contribution value of up to 28.62%. Tall and narrow building groups can provide larger shadow areas, reduce solar radiation, promote heat transfer and wind speed cycling, and effectively reduce the LST. BEI and SCD have a significant warming effect on the LST, with relative contribution values of 25.50% and 15.91%, respectively. The geometric shapes and street layouts of crowded and unevenly distributed building groups are relatively disordered, lacking fully connected ventilation corridors, affecting convective heat dissipation and causing an increase in the LST. SVF integrates building height, density, and other information, offering a more comprehensive representation of the city's internal geometric structure and sky visibility coefficient, so the impact on the thermal environment is more significant. During the day, building shading in low-visibility areas can effectively reduce solar radiation, while the ground in high-visibility areas will receive more solar radiation, which may lead to a higher LST. AV has a significant positive correlation with the LST, with a relative contribution value of 8.18%. The larger the building volume, the more human activities can be accommodated, thus generating more artificial heat sources and causing the LST to rise. PSF is negatively correlated with the LST, but the relative contribution value is only 2.68%. Although increasing the proportion of pervious surfaces can alleviate the thermal environment to a certain extent, in dense and complex urban built-up areas, pervious surfaces such as urban green spaces and bodies of water are constrained by the artificial built environment, making the cooling effect insufficient to meet the needs of urban residents.

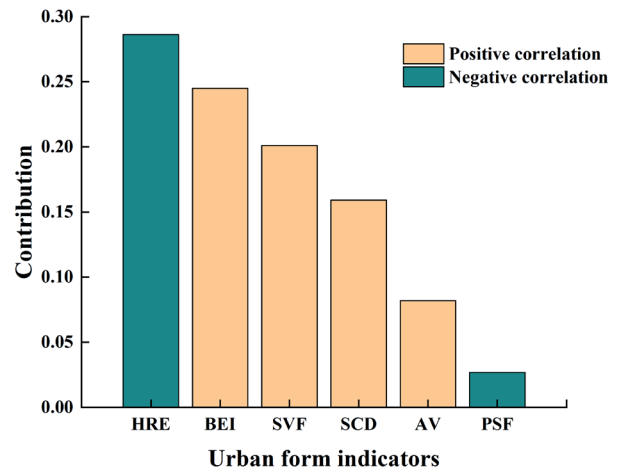


Fig. 9. Contribution of urban form indicators to LST.

Discussion

Response of Geographical Unit Division to Thermal Environment

In our investigation of the intricate relationship between urban form indicators and LST, notable variations in correlation strength and explanatory capacity were observed across distinct geographical delineation units. Specifically, employing a homogeneous grid-based methodology revealed a significant positive correlation between ISF and LST. Conversely, when transitioning to the more nuanced LCZ framework, which encapsulates factors such as building layouts, surface materials, and human activities, the correlation between ISF and LST became statistically insignificant. This observation concurs with previous research by Liu et al. [22], emphasizing that the grid's homogeneous distribution better mirrors the overall imperviousness within the respective unit. Further analysis illuminated that within the LCZ framework, both HRE and AV exhibited a notable negative correlation with LST, whereas this correlation was non-significant under the grid-based approach. This disparity stems from the fact that spatial grids tend to fragment entire buildings, failing to accurately capture the spatial heterogeneity in building height and volume. In contrast, the LCZ framework maintains a coherent spatial pattern of the landscape, affording a more precise lens for analyzing the impacts on the urban heat environment [51]. Additionally, multivariate regression analyses based on the LCZ framework produced more accurate results. This discrepancy primarily arises from the intricate distribution of buildings and the diverse land cover types within neighborhoods, necessitating a comprehensive consideration of the integrated effects of building morphology, impervious surfaces, and vegetative water bodies on the thermal environment. The

LCZ classification method, grounded in neighborhood-specific characteristics, not only preserves the integrity of landscape types but also adequately reflects the spatial heterogeneity among distinct LCZ types [52]. Consequently, this approach enables more precise predictions and improved goodness-of-fit in regression analyses. In summary, by deeply integrating factors sensitive to thermal environments, including urban structure, surface characteristics, and human activities, the LCZ theory not only enhances the quantitative description of urban spatial forms but also establishes an intrinsic link between surface morphological parameters and the urban heat island effect. This framework presents novel perspectives and avenues for crafting sustainable urban development strategies and fostering the construction of climate-resilient cities [39, 51, 53].

The Impact Mechanism of Urban Spatial Form on the Thermal Environment

Delving into the intricate interplay between LST, land cover types, and the 3D configurations of urban buildings holds paramount significance in effectively mitigating the UHI effect. Our findings reveal that, in comparison to indices such as BEI and SCD, the HRE exerts a more pronounced influence on LST, echoing the conclusions drawn by Zheng et al. [54]. This observation underscores the pivotal role played by high-rise buildings in mitigating LST by casting expansive shadows, fostering enhanced wind circulation, and facilitating heat dissipation, thereby contributing positively to the alleviation of the urban thermal environment [55]. Concurrently, the indices of SCD and BEI, which quantify the three-dimensional spatial distribution characteristics of buildings, significantly impact the distribution patterns of the thermal environment. Buildings that exhibit a uniform distribution and open spatial configurations facilitate air convection and heat transfer, thereby effectively mitigating the UHI phenomenon. SVF is an important parameter for characterizing the geometry, density, and heat balance of urban areas, and it is also an important factor for generating and controlling the heat island effect [56, 57]. This study found a significant positive correlation between SVF and LST, while Gál et al. found a strong negative correlation between LST and SVF [58]. This discrepancy may stem from the differences in spatiotemporal scales of the studies, as well as the intricacies associated with SVF's role in both solar radiation during the day and longwave radiation at night. While areas with lower SVF can provide effective shading during the day, reducing solar radiation absorption, they may also restrict the loss of longwave radiation within urban canyons during the night, delaying the surface cooling process, and thereby manifesting distinct thermal environmental effects [59]. Furthermore, the positive correlation between AV and LST reinforces the adverse effects of large-scale buildings on the intensity of the urban heat island

and thermal comfort, highlighting the significance of building energy consumption and anthropogenic heat emissions [60]. As an important parameter for characterizing height features, CH affects the coverage area and layout of building shadows and changes the surface roughness of mechanical turbulence, thus affecting the surface thermal environment. ISF and PSF are 2D morphological indicators that are closely related to the urban thermal environment; they have a significant impact on surface reflectance, the water vapor cycle, and the temperature rise and fall rates [61]. However, this study found that the correlation between ISF, PSF, and LST is weaker than that of the 3D spatial form indicators, possibly due to the greater comprehensive impact of 3D information, such as the urban canyon effect, shading effect, and building materials, on the thermal environment [11]. Therefore, in urban planning and construction, greater emphasis should be placed on the rational layout and optimal configuration of 3D building spaces to fully harness their potential in mitigating the UHI effect [62].

Limitations and Prospects

At present, although this research has made progress, some issues still need to be addressed. First of all, the spatial resolution of the LST obtained via thermal infrared remote sensing is relatively low. In the future, remote sensing technology can be combined with thermal imagers mounted on UAVs to obtain sub-meter-level LSTs, accurately reflecting the spatial complexity and details of the thermal environment at the microscale of blocks. Second, this study focuses on the analysis of factors affecting the thermal environment at the block scale. In the future, comparative studies at the regional, national, and even global scales should be conducted to explore the impact mechanisms of urban spatial morphology on the UHI at different spatial scales, in order to construct more comprehensive thermal relief measures to alleviate the LST. Third, this study only considers the quantitative relationship between summer daytime LST and urban forms and fails to fully consider the phased characteristics of thermal environmental effects in time series. In the future, it will be necessary to strengthen the comparative analysis of the impact mechanism of urban form on the thermal environment for different seasons and time scales. Finally, in the future, research on the relationship between thermal comfort, temperature, and human health should be strengthened. Using on-site measurements, questionnaire surveys, indicator evaluations, and other methods, the thermal comfort of residents should be quantified, and the mechanisms of the impact of urban spatial forms on thermal comfort should be studied.

Conclusions

This study builds on existing research to propose a more targeted street-scale LCZ scheme, thoroughly exploring the complex relationship between spatial heterogeneity of geographic units and their thermal environment responses. Furthermore, it innovatively incorporates MSPA methods to accurately identify core heat island patches and critical nodes that have a significant influence on the heat island effect. The main conclusions are as follows:

(1) The core area and the edge area account for the largest proportion of the heat island landscape, and the accumulation, diffusion, and radiation of the two areas lead to the increasing degree of aggregation among the heat island patches, which has an important impact on the spatial distribution pattern of the heat island. Using the MSPA method to study the spatial characteristics of the UHI, we can accurately identify the core heat island patches and key nodes that have a significant impact on the thermal environment. By blocking the connection of the network structure, targeted heat evacuation strategies are formulated to control and mitigate the UHI.

(2) Spatial heterogeneity and scale effects determine the different response rules of different geographical unit division methods in relation to thermal environmental effects. An LCZ based on block unit divisions can retain more complete landscape types and fully reflect the spatial heterogeneity among different LCZ types. Therefore, more accurate goodness-of-fit and analysis results can be obtained in the regression analysis. LCZ units are thus more suitable for quantitative descriptions of block-scale surface morphology parameters and correlation analyses of thermal environmental spatial characteristics.

(3) The spatial form of blocks has a significant influence on changes in the LST. The three indicators with the largest relative contribution value are HRE, BEI, and SVF. Tall buildings can provide larger shadows, an evenly distributed building layout will promote the formation of ventilation corridors, and the sky viewing angle will affect the absorption intensity of solar radiation. Urban spatial planning should focus on the influence of these indicators on LST, so as to mitigate the urban heat island effect as much as possible.

Acknowledgments

This research was funded by the Open Fund of the Key Laboratory of Geographic Information Science (Ministry of Education), and East China Normal University (No. KLGIS2021A02), the Shandong Natural Science Foundation (No. ZR2022MD070).

Data Availability Statement

The datasets used or analyzed during the current study are available from the corresponding author upon reasonable request.

Conflict of Interest

All authors declare that they have no known competing financial interests or personal relationships that could have appeared to influence the work reported in this paper.

Author Contribution

Jiayun Wang: software, formal analysis, visualization, writing—original draft, methodology, writing—review and editing. Fei Meng: conceptualization, methodology, validation, resources, supervision, funding acquisition. Tingting Jing: project administration, supervision. Lifan Qi.: investigation, validation, methodology. All authors have read and agreed to the published version of the manuscript.

References

1. YUAN B., ZHOU L., DANG X., SUN D., HU F., MU H. Separate and combined effects of 3D building features and urban green space on land surface temperature. *Journal of Environmental Management*, **295**, 113116, **2021**.
2. BERISHA A. Solar and Human Activity Impact on High and Low Land River Flows. *Civil Engineering Journal*, **9**, 1630, **2023**.
3. POUR S.H., WAHAB A.K.A., SHAHID S., ASADUZZAMAN M., DEWAN A. Low impact development techniques to mitigate the impacts of climate-change-induced urban floods: Current trends, issues and challenges. *Sustainable Cities and Society*, **62**, 102373, **2020**.
4. LI X., ZHOU W. Optimizing urban greenspace spatial pattern to mitigate urban heat island effects: Extending understanding from local to the city scale. *Urban Forestry & Urban Greening*, **41**, 255, **2019**.
5. NOYES P.D., MCELWEE M.K., MILLER H.D., CLARK B.W., VAN TIEM L.A., WALCOTT K.C., ERWIN K.N., LEVIN E.D. The toxicology of climate change: Environmental contaminants in a warming world. *Environment International*, **35** (6), 971, **2009**.
6. HE B.-J., ZHAO D., DONG X., XIONG K., FENG C., QI Q., DARKO A., SHARIFI A., PATHAK M. Perception, physiological and psychological impacts, adaptive awareness and knowledge, and climate justice under urban heat: A study in extremely hot-humid Chongqing, China. *Sustainable Cities and Society*, **79**, 103685, **2022**.
7. PATZ J.A., CAMPBELL-LENDRUM D., HOLLOWAY T., FOLEY J.A. Impact of regional climate change on human health. *Nature*, **438** (7066), 310, **2005**.
8. EBI K.L., CAPON A., BERRY P., BRODERICK C., DE DEAR R., HAVENITH G., HONDA Y., KOVATS

- R.S., MA W., MALIK A., MORRIS N.B., NYBO L., SENEVIRATNE S.I., VANOS J., JAY O. Hot weather and heat extremes: health risks. *Lancet*, **398** (10301), 698, **2021**.
9. CENTRE C.C.C. Blue Book on Climate Change in China (2022). Beijing: Science Press, **2022**.
 10. YANG X., XU X., WANG Y., YANG J., WU X. Heat exposure impacts on urban health: A meta-analysis. *Science of The Total Environment*, **947**, 174650, **2024**.
 11. LUO X., YANG J., SUN W., HE B. Suitability of human settlements in mountainous areas from the perspective of ventilation: A case study of the main urban area of Chongqing. *Journal of Cleaner Production*, **310**, 127467, **2021**.
 12. TIAN Y., ZHOU W., QIAN Y., ZHENG Z., YAN J. The effect of urban 2D and 3D morphology on air temperature in residential neighborhoods. *Landscape Ecology*, **34** (5), 1161, **2019**.
 13. AL-ABAYECHI Y.F., AL-KHAFAJI A.S. Forecasting the Impact of the Environmental and Energy Factor to Improve Urban Sustainability by Using (SEM). *Civil Engineering Journal*, **9** (10), **2023**.
 14. THANAPONGPOPN A., SAENGCHOTE K., GOWANIT C. Factors Shaping Thai Millennials' Low-Carbon Behavior: Insights from Extended Theory of Planned Behavior. *HighTech and Innovation Journal*, **4**, 482, **2023**.
 15. ZHOU W.Q., TIAN Y. Effects of urban three-dimensional morphology on thermal environment: a review. *Acta Ecologica Sinica*, **40** (2), 416, **2020**.
 16. VAN ESCH M.M.E., LOOMAN R.H.J., DE BRUINHORDIJK G.J. The effects of urban and building design parameters on solar access to the urban canyon and the potential for direct passive solar heating strategies. *Energy and Buildings*, **47**, 189, **2012**.
 17. VAN VLIET J. Direct and indirect loss of natural area from urban expansion. *Nature Sustainability*, **2** (8), 755, **2019**.
 18. CHEN Q., CHENG Q.H., CHEN Y.H. Analysis of the influence of the urban building skyview factor on landsurface thermal environment. *Science of Surveying and Mapping*, **46** (8), 148, **2021**.
 19. YAMAGUCHI Y., SHIMODA Y., MIZUNO M. Transition to a sustainable urban energy system from a long-term perspective: Case study in a Japanese business district. *Energy and Buildings*, **39** (1), 1, **2007**.
 20. LIU L., PAN X., JIN L., LIU L., LIU J. Association analysis on spatiotemporal characteristics of block-scale urban thermal environments based on a field mobile survey in Guangzhou, China. *Urban Climate*, **42**, 101131, **2022**.
 21. CHEN Y., YANG J., YANG R.X., XIAO X.M., XIA J.H. Contribution of urban functional zones to the spatial distribution of urban thermal environment. *Building And Environment*, **216**, **2022**.
 22. LIU S.Z., XIE M.M., WU R.R., WANG Y.N., LI X.Y. Influence of the choice of geographic unit on the response of urban thermal environment: Taking Beijing as an example. *Progress in Geography*, **40** (6), 1037, **2021**.
 23. XIAO H., KOPECKÁ M., GUO S., GUAN Y., CAI D., ZHANG C., ZHANG X., YAO W. Responses of Urban Land Surface Temperature on Land Cover: A Comparative Study of Vienna and Madrid. *Sustainability*, **10** (2), **2018**.
 24. STEWART I.D., OKE T.R. Local Climate Zones for Urban Temperature Studies. *Bulletin of the American Meteorological Society*, **93** (12), 1879, **2012**.
 25. ALEXANDER P.J., MILLS G., FEALY R. Using LCZ data to run an urban energy balance model. *Urban Climate*, **13**, 14, **2015**.
 26. FERNANDES R., NASCIMENTO V., FREITAS M., OMETTO J. Local Climate Zones to Identify Surface Urban Heat Islands: A Systematic Review. *Remote Sensing*, **15** (4), **2023**.
 27. BECHTEL B., ALEXANDER P.J., BÖHNER J., CHING J., CONRAD O., FEDDEMA J., MILLS G., SEE L., STEWART I. Mapping Local Climate Zones for a Worldwide Database of the Form and Function of Cities. *Geo-Information*, **4** (1), 199, **2015**.
 28. CAI M., REN C., XU Y., DAI W., WANG X.M. Local Climate Zone Study for Sustainable Megacities Development by Using Improved WUDAPT Methodology – A Case Study in Guangzhou. *Procedia Environmental Sciences*, **36**, 82, **2016**.
 29. GÁL T., BECHTEL B., LELOVICS E. Comparison of two different Local Climate Zone mapping methods. In: 9th International Conference on Urban Climates (ICUC9), Toulouse, France, **2015**.
 30. BROUSSE O., MARTILLI A., FOLEY M., MILLS G., BECHTEL B. WUDAPT, an efficient land use producing data tool for mesoscale models? Integration of urban LCZ in WRF over Madrid. *Urban Climate*, **17**, 116, **2016**.
 31. MA Y.H., LU L.L., XIAO D., CAI M., REN C., ZHOU M.L., HUI W.H., LI Q.T. Urban thermal environment analysis by local climate zone in Beijing. *Journal of Beijing Normal University (Natural Science)*, **58** (06), 901, **2022**.
 32. WANG R., REN C., XU Y., LAU K.K.-L., SHI Y. Mapping the local climate zones of urban areas by GIS-based and WUDAPT methods: A case study of Hong Kong. *Urban Climate*, **24**, 567, **2018**.
 33. QUAN S.J., DUTT F., WOODWORTH E., YAMAGATA Y., YANG P.P.-J. Local Climate Zone Mapping for Energy Resilience: A Fine-grained and 3D Approach. *Energy Procedia*, **105**, 3777, **2017**.
 34. PERERA N.G.R., EMMANUEL R. A “Local Climate Zone” based approach to urban planning in Colombo, Sri Lanka. *Urban Climate*, **23**, 188, **2018**.
 35. YIN C., YUAN M., LU Y., HUANG Y., LIU Y. Effects of urban form on the urban heat island effect based on spatial regression model. *Science of the Total Environment*, **634**, 696, **2018**.
 36. KUANG W.H., YANG T.R., LIU A.L., ZHANG C., LU D.S., CHI W.F. An EcoCity model for regulating urban land cover structure and thermal environment: Taking Beijing as an example. *Science China-Earth Sciences*, **60** (6), 1098, **2017**.
 37. KONG F.H., CHEN J.Y., MIDDEL A., YIN H.W., LI M.C., SUN T., ZHANG N., HUANG J., LIU H.Q., ZHOU K.J., MA J.S. Impact of 3-D urban landscape patterns on the outdoor thermal environment: A modelling study with SOLWEIG. *Computers Environment And Urban Systems*, **94**, **2022**.
 38. SVENSSON M.K. Sky view factor analysis – implications for urban air temperature differences. *Meteorological Applications*, **11** (3), 201, **2004**.
 39. JIN L., PAN X., LIU L., LIU L., LIU J., GAO Y. Block-based local climate zone approach to urban climate maps using the UDC model. *Building and Environment*, **186**, 107334, **2020**.
 40. WENG Q., LU D., SCHUBRING J. Estimation of land surface temperature–vegetation abundance relationship for urban heat island studies. *Remote Sensing of Environment*, **89** (4), 467, **2004**.

41. MORAN P.A.P. The Interpretation of Statistical Maps. *Journal of the Royal Statistical Society: Series B (Methodological)*, **10** (2), 243, **1948**.
42. ANSELIN L. Local Indicators of Spatial Association—LISA. *Geographical Analysis*, **27** (2), 93, **1995**.
43. VOGT P., RIITERS K.H., ESTREGUIL C., KOZAK J., WADE T.G., WICKHAM J.D. Mapping Spatial Patterns with Morphological Image Processing. *Landscape Ecology*, **22** (2), 171, **2007**.
44. CHEN S.L., WANG T.X. Comparison analyses of equal interval method and mean-standard deviation method used to delimitate urban heat island. *Journal of Geoinformation Science*, **11** (02), 145, **2009**.
45. JIANG Y.H., JIAO L.M., ZHANG B.E. Scale effect of the spatial correlation between urban land surface temperature and NDVI. *Progress in Geography*, **37** (10), 1362, **2018**.
46. YV X.Y., XV G., LIU Y., XIAO R. Influences of 3D features of buildings on land surface temperature: A case study in the Yangtze River Delta urban agglomeration. *China Environmental Science*, **041** (012), 5806, **2021**.
47. LUO P.Y., YU B.J., LI P.F., LIANG P.P., LIANG Y., YANG L.C. How 2D and 3D built environments impact urban surface temperature under extreme heat: A study in Chengdu, China. *Building And Environment*, **231**, **2023**.
48. CURTO J.D., PINTO J.C. The corrected VIF (CVIF). *Journal Of Applied Statistics*, **38** (7), 1499, **2011**.
49. YIN C.H., YUAN M., LU Y.P., HUANG Y.P., LIU Y.F. Effects of urban form on the urban heat island effect based on spatial regression model. *Science Of The Total Environment*, **634**, 696, **2018**.
50. XV, H.Q. Dynamic of exposed bare soils and its impact on local thermal environment. *Transactions of the CSA*, **28** (23), 98, **2012**.
51. LEHNERT M., SAVIC S., MILOSEVIC D., DUNJIC J., GELETIC J. Mapping Local Climate Zones and Their Applications in European Urban Environments: A Systematic Literature Review and Future Development Trends. *ISPRS International Journal Of Geo-Information*, **10** (4), **2021**.
52. PENG F., CAO Y.W., SUN X.Q., ZOU B. Study on the contributions of 2D and 3D urban morphologies to the thermal environment under local climate zones. *Building And Environment*, **263**, **2024**.
53. XUE J., YOU R.Y., LIU W., CHEN C., LAI D.Y. Applications of Local Climate Zone Classification Scheme to Improve Urban Sustainability: A Bibliometric Review. *Sustainability*, **12** (19), **2020**.
54. ZHENG Z., ZHOU W., YAN J., QIAN Y., WANG J., LI W. The higher, the cooler? Effects of building height on land surface temperatures in residential areas of Beijing. *Physics and Chemistry of the Earth, Parts A/B/C*, **110**, 149, **2019**.
55. CAI H., XU X. Impacts of Built-Up Area Expansion in 2D and 3D on Regional Surface Temperature. *Sustainability*, **9** (10), **2017**.
56. LAI A., MAING M., NG E. Observational studies of mean radiant temperature across different outdoor spaces under shaded conditions in densely built environment. *Building and Environment*, **114** 397, **2017**.
57. MENG F., YU Q., YANG X. Analysis of Influence of Urban Spatial Morphologies on Thermal Microenvironment. *Polish Journal of Environmental Studies*, **30** (2), 1725, **2021**.
58. GÁL T., LINDBERG F., UNGER J. Computing continuous sky view factors using 3D urban raster and vector databases: comparison and application to urban climate. *Theoretical and Applied Climatology*, **95** (1), 111, **2009**.
59. PARK S., PARK J., LEE S. Unpacking the nonlinear relationships and interaction effects between urban environment factors and the urban nighttime heat index. *Journal Of Cleaner Production*, **428**, **2023**.
60. ISA N.A., SALLEH S.A., MOHD W., CHAN A., OOI M.C.G., ZAKARIA N.H., ISLAM M.A. IOP Building Volume Effects on Ambient Temperature In The Kuala Lumpur City. *IOP Conference Series: Earth and Environmental Science*, **489**, 012011, **2020**.
61. XU H.Q., LIN D.F., TANG F. The impact of impervious surface development on land surface temperature in a subtropical city: Xiamen, China. *International Journal Of Climatology*, **33** (8), 1873, **2013**.
62. WANG J., MENG F., FU P., JIN F. Investigating the Coupling of Supply and Demand for Urban Blue and Green Spaces’ Cooling Effects in Shandong, China, **14** (2), 404, **2023**.